(c)1999 American Institute of Aeronautics & Astronautics

A99-16124

AIAA 98–0200

LES of Turbulent Fuel/Air Mixing in a Swirling Combustor

Won-Wook Kim and Suresh Menon
School of Aerospace Engineering
Georgia Institute of Technology
Atlanta, Georgia 30332-0150

37th AIAA Aerospace Sciences Meeting and Exhibit
January 11–14, 1999 / Reno, NV

For permission to copy or republish, contact the American Institute of Aeronautics and Astronautics
1801 Alexander Bell Drive, Suite 500, Reston, VA 22191–4344

(c)1999 American Institute of Aeronautics & Astronautics

LES of Turbulent Fuel/Air Mixing in a Swirling Combustor

Won-Wook Kim* and Suresh Menon†
School of Aerospace Engineering
Georgia Institute of Technology
Atlanta, Georgia 30332-0150

Large-eddy simulation (LES) of turbulent fuel/air mixing in a gas turbine combustor that is a close approximation of a lean premixed combustor under development at General Electric Aircraft Engine Company has been carried out to quantify the efficiency of the premixer of this combustor. Experimental studies show that the swirling fuel/air mixture generated by the dual annular counter-rotating premixer has significant spatial variation in the local equivalence ratio in the near field. This unmixedness can impact the emission characteristics of the combustor. The present study is focussed on determining if this observed phenomenon can be captured in a numerical simulation that accurately captures the dynamics of scalar mixing within the context of a conventional LES. Results discussed in this paper demonstrate the ability of the LES methodology to not only capture the unmixedness observed in the experiments but also to provide detailed information related to the scalar properties. Some limitations of the conventional scalar subgrid closure are identified and possible solutions are also proposed.

1 Introduction

Turbulent mixing of chemical species involves two separate physical processes that work concurrently. The first process is turbulent convective stirring and the second is molecular diffusion. In turbulent stirring, the interface between (initially separate) reactants are convoluted by the action of turbulent eddies. These eddies distort the interfacial surface on length scales which range from the largest scale of turbulence down to the Kolmogorov microscale. Surface distortion results in large increase in the interfacial area and in the local species gradients. This process of turbulent stirring does not mix the reactant species but only distorts the surface between them. Molecular diffusion, on the other hand, is the process by which species are mixed at the molecular level. In turbulent flows, molecular diffusion is dominated by inertial forces and is essentially negligible except at the smallest scales. At these scales, species gradients become sufficiently large so that molecular diffusion becomes important.

To obtain accurate results from a numerical simulation requires accurate modeling of the turbulent mixing process. This issue is the primary focus of the present study. In particular, we study the mixing process in a dry low-emission premixer which is a part of an operational LM-6000 lean premixed combustor being developed by General Electric Aircraft Engine (GEAE) Company for gas turbine applications. The mixing efficiency of the dual annular counter-rotating swirler premixer is also being evaluated experimentally.[1] The extent of premixing achieved by the premixer is very important to quantify since variation in the local equivalence ratio can increase the NOx emission levels[2] and, especially in the lean case, result in combustion instability.[3] In the aforementioned experimental study, quantitative maps of the spatial and temporal fuel/air distribution downstream of the premixer were obtained using planar laser-induced fluorescence (PLIF). Time-averaged results showed a maximum spatial variation on the order of 50% of the known overall equivalence ratio and temporal unmixedness in peak equivalence ratio 2.4 times larger than the overall stoichiometry was observed in the experimental data. Thus, it is clear that the configuration has significant variation in the mixedness.

To determine if this unmixedness can be numerically predicted, we study the identical mixing problem using currently available large-eddy simulation(LES) methodology. The underlying philosophy behind LES is to explicitly calculate the large energy containing scales of motion which are directly affected by boundary conditions while modeling only the small scales of the flow. The large scales are difficult to model due to their variability from one problem geometry to the next. The smaller scales are presumed to be more universal in nature and, therefore, more amenable to successful modeling. The LES equations of motion describe the evolution of the large scales and are derived by applying a *spatial* filter function to the gas-phase, Navier-Stokes reacting flow equations. This filtering process separates out the effects of the geometry dependent large scales from the more universal small scales. The effect of the small unresolved scales appears as additional unknown subgrid terms in the

*Post-Doctoral Fellow, AIAA Member
†Professor, AIAA Senior Member

Copyright © 1999 by Won-Wook Kim and Suresh Menon. Published by the American Institute of Aeronautics and Astronautics, Inc. with permission.

(c)1999 American Institute of Aeronautics & Astronautics

large-scale or resolved field equations. These subgrid terms must be modeled or additional equations for these terms derived in order to close the LES equations.

One attractive aspect of LES is that the dynamics of much of the turbulent motions are captured without modeling. LES is therefore expected to provide a much more realistic picture of turbulent interactions than is obtained from Reynolds-Averaged Navier-Stokes Simulations (RANS) where all turbulence scales are modeled. LES is also not as restricted by temporal and spatial resolution requirements as is Direct Numerical Simulation (DNS) where all turbulence scales are directly resolved without employing any models. LES may therefore be applied to high Reynolds number flows of general interest which are unattainable using DNS. Consequently, LES appears to be an excellent compromise between the strengths and weakness of the DNS and RANS approaches. Furthermore, as demonstrated by Kim *et al.*,[4] for practical application to engineering flows of interest the typical grid resolution for reasonable turnaround is much coarser than suggested by classical algebraic subgrid closures. As a result, engineering LES requires use of higher order subgrid models even of closure of the subgrid stresses.[5,6]

When the concept of LES is extended to the simulation of scalar turbulent mixing, some fundamentally different considerations need to be considered. As noted above, stirring by the turbulent eddies must be accompanied by molecular diffusion to achieve mixing of species. Thus, accurate modeling of mixing at the small scales and the subsequent molecular diffusion effects is critical to the prediction of local mixedness. However, in conventional LES, when eddy-diffusivity subgrid closure (which is based on analogous arguments used for the closure of the subgrid stresses using the eddy viscosity) is employed then it is implicitly assumed that *both* the fine scale mixing effects (i.e., stirring at the subgrid scales and molecular diffusion) can be adequately modeled by an effective diffusivity that scales with the subgrid eddy viscosity. This assumption is not truly justifiable; however, it has not yet been established what are the quantifiable errors inherent in this approach. For example, if the inflow is assumed to be fully premixed, then under certain conditions (i.e., appropriate Reynolds and Damkohler numbers) the flamelet model is applicable. Then, the conventional G-equation LES approach can be employed with reasonable accuracy for engineering predictions as recently demonstrated.[4] However, when turbulent mixing efficiency has to be predicted, conventional closure needs to be evaluated for accuracy within the constraints of an engineering LES. Failure of this type of closure would indicate the need for a subgrid scalar closure that accounts for the small scale turbulent stirring and molecular diffusion processes using methodology recently demonstrated.[7-9]

This paper addresses these issues using a problem of engineering (i.e., practical) interest using LES resolution that is practically feasible on available processing systems.

2 LES Governing Equations

The Navier-Stokes equations that govern the conservation of mass, momentum, and energy in a fluid, are filtered to obtain the LES equations for fluid motions. The filtering operation results in terms that must be modeled. The relevant equations for LES of turbulent premixed reacting flows are summarized here.

The continuum equations of motion for a compressible, multi-species, reacting fluid are the Navier-Stokes equations describing the conservation of mass, momentum, total energy, and chemical species:

$$\begin{aligned}
&\frac{\partial \rho}{\partial t} + \frac{\partial \rho u_i}{\partial x_i} = 0 \\
&\frac{\partial \rho u_i}{\partial t} + \frac{\partial}{\partial x_j}[\rho u_i u_j + p\delta_{ij} - \tau_{ij}] = 0 \\
&\frac{\partial \rho E}{\partial t} + \frac{\partial}{\partial x_i}[(\rho E + p)u_i + q_i - u_j \tau_{ij}] = 0 \\
&\frac{\partial \rho Y_m}{\partial t} + \frac{\partial}{\partial x_i}[\rho Y_m (u_i + V_{i,m})] = \dot{w}_m \qquad m = 1, N-1
\end{aligned} \tag{1}$$

written in Cartesian tensor form. In the above equations, t is the time, ρ is the mass density, p is the pressure, E is the total energy per unit mass, x_i $(i = 1, 2, 3)$ is the coordinate, u_i is the velocity vector, q_i is the heat flux vector, and δ_{ij} is the Kronecker delta. The individual species mass fraction, diffusion velocities, and mass reaction rate per unit volume are, respectively, Y_m, $V_{i,m}$, and $\dot{w}_m$. The viscous stress tensor is given by $\tau_{ij} = \mu(\partial u_i/\partial x_j + \partial u_j/\partial x_i) - \frac{2}{3}\mu(\partial u_k/\partial x_k)\delta_{ij}$ where μ is the molecular viscosity coefficient and it is approximated using Sutherland's Law. The pressure is determined from the equation of state for a perfect gas mixture

$$P = \rho T \sum_{m=1}^{N} Y_m R_u / W_m \tag{2}$$

where T is the temperature, R_u is the universal gas constant, and W_m the individual molecular weight. The total energy per unit volume is determined from $\rho E = \rho(e + \frac{1}{2}u_k^2)$ where e is the internal energy per unit mass given by $e = \sum_{m=1}^{N} Y_m h_m - P/\rho$ and h_m is the individual enthalpy. The diffusion velocities are approximated by Fickian diffusion, $V_{i,m} = (-D_m/Y_m)(\partial Y_m/\partial x_i)$ where D_m is the mixture averaged molecular diffusion coefficient. The caloric equation of state is given by,

$$h_m = \Delta h^0_{f,m} + \int_{T^0}^{T} c_{p,m}(T')dT' \tag{3}$$

where $\Delta h^0_{f,m}$ is the standard heat of formation at temperature T^0 and $c_{p,m}$ is the individual specific heat at constant pressure.

(c)1999 American Institute of Aeronautics & Astronautics

Finally, the species mass fractions, diffusion velocities and molar fractions are constrained by the following identities:

$$\sum_{m=1}^{N} Y_m = 1, \quad \sum_{m=1}^{N} V_{i,m} = 0, \quad X_m = \frac{(Y_m/W_m)}{\sum_{n=1}^{N}(Y_m/W_m)}. \tag{4}$$

Spatial filtering reduces the high wave number Fourier components of the flow variables and separates the resolved scale components from the unresolved scales. Following Erlebacher *et al.*,[10] the flow variables are decomposed into the resolved (supergrid scale) and unresolved (subgrid scale) components by a spatial filtering operation such that $f = \widetilde{f} + f''$, where the ($\sim$) denotes resolved and ($''$) denotes subgrid quantities. The Favre filtered variable is defined as,

$$\widetilde{f} = \frac{\overline{\rho f}}{\overline{\rho}} \tag{5}$$

where the over bar represents a spatial filtering which is defined as,

$$\overline{f(x_i,t)} = \int f(x_i^{'},t) G_f(x_i, x_i^{'}) dx_i^{'}. \tag{6}$$

Here, G_f is the filter kernel and the integral is extended over the entire domain. Applying the filtering operation (in the present study, a low-pass filter of the computational mesh is used, hence, the characteristic size of this filter is the grid width $\overline{\Delta}$) to the Navier-Stokes equations, the following LES equations for mass, momentum, and energy are obtained:

$$\begin{aligned}
&\tfrac{\partial \overline{\rho}}{\partial t} + \tfrac{\partial \overline{\rho}\widetilde{u}_i}{\partial x_i} = 0 \\
&\tfrac{\partial \overline{\rho}\widetilde{u}_i}{\partial t} + \tfrac{\partial}{\partial x_j}[\overline{\rho}\widetilde{u}_i\widetilde{u}_j + \overline{p}\delta_{ij} - \overline{\tau}_{ij} + \tau_{ij}^{sgs}] = 0 \\
&\tfrac{\partial \overline{\rho}\widetilde{E}}{\partial t} + \tfrac{\partial}{\partial x_i}[(\overline{\rho}\widetilde{E} + \overline{p})\widetilde{u}_i + \overline{q}_i - \widetilde{u}_j\overline{\tau}_{ij} + H_i^{sgs} + \sigma_{ij}^{sgs}] = 0 \\
&\tfrac{\partial \overline{\rho}\widetilde{Y}_m}{\partial t} + \tfrac{\partial}{\partial x_i}[\overline{\rho}\widetilde{Y}_m\widetilde{u}_i - \overline{\rho}\bar{D}_m \tfrac{\partial \widetilde{Y}_m}{\partial x_i} + \Phi_{i,m}^{sgs}] = \overline{\dot{w}}_m
\end{aligned} \tag{7}$$

where, and $\overline{\tau}_{ij}$ and $\overline{q}_i$ are approximated simply in terms of the filtered velocity. The unclosed subgrid terms representing respectively, the subgrid stress tensor, subgrid heat flux, unresolved viscous work, species mass flux, and filtered reaction rate are:

$$\begin{aligned}
\tau_{ij}^{sgs} &= \overline{\rho}[\widetilde{u_i u_j} - \widetilde{u}_i\widetilde{u}_j] \\
H_i^{sgs} &= \overline{\rho}[\widetilde{E u_i} - \widetilde{E}\widetilde{u}_i] + [\overline{p u_i} - \overline{p}\widetilde{u}_i] \\
\sigma_i^{sgs} &= [\overline{u_j \tau_{ij}} - \widetilde{u}_j\overline{\tau}_{ij}] \\
\Phi_{i,m}^{sgs} &= \bar{\rho}[\widetilde{u_i Y_m} - \tilde{u}_i\tilde{Y}_m] \\
\overline{\dot{w}}_m &
\end{aligned} \tag{8}$$

3 SUBGRID MODELING

Closure of the filtered governing equations can be achieved using subgrid models. In the present study, the localized dynamic model based on the subgrid turbulent kinetic energy is employed for subgrid turbulence modeling. Subgrid closure for turbulent scalar mixing is based on an eddy diffusivity model which is related to the dynamic eddy viscosity. In this section, these models are summarized.

3.1 Momentum and Energy Transport Closure

In this study, a compressible version of the localized dynamic model introduced by Kim and Menon[9] is employed. This model is based on the subgrid kinetic energy which is solved by the following transport equation:[11]

$$\frac{\partial \overline{\rho} k^{sgs}}{\partial t} + \frac{\partial}{\partial x_i}(\overline{\rho}\widetilde{u}_i k^{sgs}) = P^{sgs} - D^{sgs} + \frac{\partial}{\partial x_i}\left(\frac{\overline{\rho}\nu_t}{Pr_t}\frac{\partial k^{sgs}}{\partial x_i}\right) \tag{9}$$

where $k^{sgs} = \frac{1}{2}[\widetilde{u_k^2} - \widetilde{u}_k^2]$ is the subgrid kinetic energy and Pr_t is the turbulent Prandtl number. The subgrid turbulence intensity is related to k^{sgs} by $u_{sgs}^{'} = \sqrt{\frac{2}{3}k^{sgs}}$. The terms on the right side of equation (9) represent, respectively, the production, the dissipation, and the transport of the subgrid kinetic energy. The production term is modeled as $P^{sgs} = -\tau_{ij}^{sgs}(\partial\widetilde{u}_i/\partial x_j)$ where the subgrid shear stresses τ_{ij}^{sgs} are evaluated as,

$$\tau_{ij}^{sgs} = -2\overline{\rho}\nu_t(\widetilde{S}_{ij} - \frac{1}{3}\widetilde{S}_{kk}\delta_{ij}) + \frac{2}{3}\overline{\rho}k^{sgs}\delta_{ij}. \tag{10}$$

Here, ν_t is the subgrid eddy viscosity given by $\nu_t = C_\nu(k^{sgs})^{1/2}\overline{\Delta}$ and $\widetilde{S}_{ij} = \frac{1}{2}(\partial\widetilde{u}_i/\partial x_j + \partial\widetilde{u}_j/\partial x_i)$ is the resolved-scale rate-of-strain tensor. The dissipation term is modeled as $D^{sgs} = C_\epsilon\overline{\rho}(k^{sgs})^{3/2}/\overline{\Delta}$, where, $\overline{\Delta}$ is a characteristic grid size. The two coefficients appearing in the above equations, C_ν and C_ϵ are determined dynamically. In the following, the localized dynamic k-equation model (denoted here as the LDKM) is briefly summarized.

As in other dynamic models,[12] the LDKM is also based on the assumption of scale similarity in the inertial subrange. Provided that enough of the inertial subrange is resolved, stresses at the cutoff (i.e., the grid size) can be related to stresses at say twice the cutoff (i.e., the test filter width). This then defines a scale level where explicit filtering is required. The test-scale field is constructed from the grid-scale field by applying a test filter which is characterized by $\widehat{\Delta}$ (typically, $\widehat{\Delta} = 2\overline{\Delta}$). A test filter shape which is consistent with the grid filter in form is preferred. Some researchers[13,14] have investigated the effect of various filter shapes on the turbulence statistics. However, the optimal choice (in terms of accuracy and efficiency) of filters for a particular numerical method has not yet been established. In the present study, the top-hat filter based on the trapezoidal rule is employed for the test filter. This filter is consistent with finite-volume methods[15] and is implicit in the grid filter. If the application of the test filter on any variable o is denoted by $\widehat{\phi}$ and the test-scale Favre-filtered variable is denoted by $< \phi >= \widehat{\overline{\rho}\phi}/\widehat{\overline{\rho}}$, the test-scale Leonard stress

(c)1999 American Institute of Aeronautics & Astronautics

tensor can be defined as:

$$L_{ij} = \widehat{\overline{\rho}} \left(\langle \widetilde{u}_i \widetilde{u}_j \rangle - \langle \widetilde{u}_i \rangle \langle \widetilde{u}_j \rangle \right). \tag{11}$$

At the test-filter level, a resolved kinetic energy can be defined from the trace of equation (11): $k^{test} = \frac{1}{2} \left(\langle \widetilde{u}_k \widetilde{u}_k \rangle - \langle \widetilde{u}_k \rangle \langle \widetilde{u}_k \rangle \right)$ (note that $k^{test} = \frac{1}{2} L_{kk} / \widehat{\overline{\rho}}$). This energy is similar to k^{sgs}, however, it is produced at the large scales by $-L_{ij}(\partial < \widetilde{u}_i > / \partial x_j)$ and is dissipated by: $D^{test} = \mu' \left(\langle \overline{\tau}_{ij} \partial \widetilde{u}_i / \partial x_j \rangle - \langle \overline{\tau}_{ij} \rangle \langle \partial \widetilde{u}_i / \partial x_j \rangle \right)$ at the small scales. Here, $\mu' = (\mu + \overline{\rho} \nu_t) / \mu$ is multiplied since k^{test} is fully resolved at the test-filter level and, thus, must be dissipated by both the eddy viscosity and the molecular viscosity.

Liu *et al.*[16] observed significant similarity between τ_{ij}^{sgs} and L_{ij} in their experimental data obtained in the far field of a turbulent round jet at reasonably high Reynolds number, $Re_\lambda \approx 310$ (Re_λ is the Reynolds number defined based on turbulence intensity and Taylor microscale λ). The experimental data showed that the correlation between these two stress tensors was quite high. Thus, it is reasonable to assume that similar representation can be used to represent τ_{ij}^{sgs} and L_{ij} using appropriately defined parameters. Since τ_{ij}^{sgs} is modeled in terms of grid-resolved quantities, a similar representation is considered for L_{ij} in terms of quantities which are resolved at the test-filter level:

$$L_{ij} = 2 C_\nu M_{ij} + \frac{2}{3} \widehat{\overline{\rho}} k^{test} \delta_{ij} \tag{12}$$

where $M_{ij} = -\widehat{\overline{\rho}} \sqrt{k^{test}} \widehat{\Delta} \left(\left\langle \widetilde{S}_{ij} \right\rangle - \frac{1}{3} \left\langle \widetilde{S}_{kk} \right\rangle \delta_{ij} \right)$. The resulting relation contains only C_ν as the only unknown. Thus, the relation can be viewed as an explicit model representation for C_ν in terms of quantities resolved at the test-filter level. Upon applying the least-square method suggested by Lilly[17] to this overdetermined system, C_ν is obtained as

$$C_\nu = \frac{L'_{ij} M_{ij}}{2 M_{ij} M_{ij}} \tag{13}$$

where $L'_{ij} = L_{ij} - \frac{2}{3} \widehat{\overline{\rho}} k^{test} \delta_{ij}$. This formulation can be contrasted to the classical Germano-type of dynamic closure where the mathematical identity in terms of the model representation at the two filter levels results in the denominator of equation (13) to be ill-conditioned (i.e., to tend to zero locally). As a result, some algorithmic adjustments are typically needed (e.g., spatial averaging in a homogeneous direction). The present LDKM approach avoids this problem since the denominator only contains a well defined (and nonzero) quantity.

Similarity between the dissipation rates D^{sgs} at the grid-filter level and D^{test} at the test-filter level is also invoked in the LDKM to obtain the dissipation model coefficient. Thus, we obtain $D^{test} = C_\epsilon \widehat{\overline{\rho}} (k^{test})^{3/2} / \widehat{\Delta}$. Since this equation is a single equation with one unknown, C_ϵ can be determined easily from

$$C_\epsilon = \frac{\widehat{\Delta} \mu'}{\widehat{\overline{\rho}} (k^{test})^{3/2}} \left(\left\langle \overline{\tau}_{ij}^{sgs} \frac{\partial \widetilde{u}_i}{\partial x_j} \right\rangle - \langle \overline{\tau}_{ij}^{sgs} \rangle \left\langle \frac{\partial \widetilde{u}_i}{\partial x_j} \right\rangle \right). \tag{14}$$

In summary, by assuming similarity between τ_{ij}^{sgs} and L_{ij} (which appears reasonable from experimental data), the LDKM can be formulated without employing any mathematically inconsistent or *ad hoc* procedure (the mathematical inconsistency of Germano *et al.*'s dynamic formulation has been pointed out earlier by Cabot and Moin[18]). There are some more positive aspects to this approach. As noted above, the denominators of equations (13) and (14) contain well-defined quantities (i.e., subtest kinetic energy k^{test}) and, therefore, the ill-conditioning problem (seen in Germano *et al.*'s dynamic formulation) is significantly relieved. The prolonged presence of negative model coefficient discussed by Lund *et al.*[19] also can be avoided in the present model since it is based on the subgrid kinetic energy. Moreover, the dynamically determined C_ϵ from equation (14) does not vanish in the limit of high Reynolds number (a phenomenon that was observed in an earlier dynamic kinetic energy model formulation by Wong[20]).

Analysis of results have shown that the LDKM is Galilean-invariant and satisfy well[21] the realizability conditions given by Schumann.[22] From a computational standpoint, the cost of the present dynamic procedure is not significant (about the same as Germano *et al.*'s dynamic model) due to its simplicity. The additional computational cost is primarily due to the inclusion of a transport equation for k^{sgs}. This extra computational cost can be justified since, for LES of reacting flows, the one-equation eddy-viscosity model and its derivatives are superior to the algebraic models including Germano *et al.*'s dynamic algebraic model. This issue was discussed by Fureby[23] in his recent LES review paper. For LES of nonreacting flows using reasonable grid resolutions, the effects of the subgrid model on the statistical quantities are usually marginal however it becomes significant when coarse grids are used. Kim and Menon[6] demonstrated the ability of the LDKM approach when applied to high Reynolds number flows using relatively coarse grids. Interestingly, the superior ability of the LDKM model in coarse grid LES was also demonstrated independently by Fureby *et al.*[21] in their comparative study of various subgrid models. It is worthwhile to emphasize that the LDKM is a *truly* localized dynamic model which evaluates the model coefficients locally (both in space and time) without any *ad hoc* averaging and, furthermore, this model behaves correctly near walls and in laminar flow regime without any special treatment. A more comprehensive discussion on the properties of the LDKM can be found elsewhere.[24-26]

(c)1999 American Institute of Aeronautics & Astronautics

Finally, the subgrid energy flux is approximated as: $H_i^{sgs} = -(\overline{\rho}\nu_t/Pr_t)\,\partial\widetilde{H}/\partial x_i$ where $\widetilde{H}$ is the filtered total enthalpy, $\widetilde{H} = \widetilde{E} + \overline{p}/\overline{\rho}$. The unclosed subgrid term σ_i^{sgs} is expected to be small[27] and so it is neglected in the present study.

3.2 Scalar Transport Closure

Since the present study is limited to fuel/air mixing (without heat release) only the term $\Phi_{i,m}^{sgs}$ needs to be closed. At present, this term is closed using the gradient diffusion assumption as follows:

$$\Phi_{i,m}^{sgs} = -\bar{\rho}\frac{\nu_T}{Sc_t}\frac{\partial \tilde{Y}_m}{\partial x_i} \qquad (15)$$

where Sc_t is the turbulent Schmidt number. Although Sc_t can be determined using a dynamic model, at present, it is assumed to be unity.

The magnitude of $\Phi_{i,m}^{sgs}$, as modeled in equation (15), is expected to dominate molecular diffusion in high Reynolds numbers flows when the subgrid turbulent kinetic energy is large. The effect of molecular diffusion in the filtered species equation results from the terms involving the diffusion velocities $V_{i,m}$. When $\Phi_{i,m}^{sgs}$ swamps the molecular diffusion terms, the final solution can be expected to be invariant with the diffusion process. This was found to be the case in the study of high Reynolds number jet flows modeled using the equation (15). Molecular diffusion is thereby effectively neglected in the resolved scale equation.

It should be noted that this approach is considered a first level approximation for the scalar mixing model. In the present paper, we will evaluate the ability of this type of simple closure in non-reacting fuel/air mixing flows. However, this closure is not applicable in reacting flow simulations because the combustion process is strongly dependent on molecular diffusion at the small scales. Improperly accounting for molecular diffusion may results in significant errors, especially, in the prediction of radical species distribution. The inability of this type of approximation in reacting flows has been noted in earlier studies.[28] Therefore, the present non-reacting mixing study is considered the first step towards the development of a more comprehensive simulation methodology. In fact, an alternative subgrid modeling approach which avoids this difficulty has already been proposed by Menon *et al.*[29] They investigated the application of *linear-eddy model* (LEM) as a subgrid model in LES of turbulent premixed and diffusion flames. The key feature of LEM is that it explicitly accounts for both small scale turbulent stirring and molecular diffusion as two distinct but concurrent processes that occur within every LES grid. Fully coupled LES-LEM method has been developed in recent studies.[7–9] The predictions obtained using LES-LEM to simulate the fuel/air mixing process will be reported in the near future.[30]

4 RESULTS AND DISCUSSION

In the present study, the subgrid mixing model based on the gradient diffusion assumption is evaluated by applying it to the simulation of a gas turbine combustor flow. Another numerical experiment which uses a more comprehensive subgrid mixing model based on the linear-eddy model is currently being conducted and the results will be presented elsewhere.[30]

The test problem is a partially premixed turbulent flow generated by a dry low-emission premixer which is a part of an operational LM-6000 lean premixed combustor being developed by GEAE for gas turbine applications.[31] The fuel/air premixer used in the experimental study[1] was a dual annular counter-rotating swirler premixer.[32] A centerline sectional view of the gas turbine combustor is shown in Figure 1. The premixer exit (i.e., combustor inlet) diameter is 48mm and the combustor has a 129mm diameter. Therefore, the increase in cross-sectional area over the backward facing step of the dump combustor is 7.2:1. A swirling jet (the maximum value of tangential velocity component is slightly greater than the peak value of axial velocity component) is injected from the premixer under conditions of pressure=$1.16\text{x}10^5$ N/m^2 and temperature=350 K. The swirl number $S = \int_0^R \rho u w r^2 dr / R\int_0^R \rho u^2 r dr$. was about 0.56. This swirl number belongs to the regime where onset of an internal recirculation zone (IRZ; this is also known as a vortex breakdown) occurs.[4] The radial number $R = \int_0^R \rho u v r dr / \int_0^R \rho u^2 r dr$ which represents the effect of inlet radial velocity was 0.012. The Reynolds number Re based on the inlet mean streamwise velocity and the inlet jet diameter D_0, is 330,000. Figure 1 also shows a layout of the positions chosen for histogram analysis in Figure 6.

The present LES was implemented using a finite-volume code that is fourth-order accurate in space and second-order accurate in time. The full compressible LES equations are solved (along with the subgrid kinetic energy equation) in Cartesian coordinates. The 3-dimensional computational grid was generated by rotating the 2-dimensional grid with respect to the combustor centerline and the actual grid used for the present study is shown in Figure 2. This manner of grid generation has been employed to efficiently cluster the grid points near the jet shear layer whose resolution is critical since most of important turbulent processes occur there. The grid has $101 \times 61 \times 81$ grid points along, respectively, axial, radial, and azimuthal directions (only every other grid points in each direction are shown in the plot for a better presentation). This resolution is considered very coarse and not representative of typical LES reported in the literature. However, this resolution was chosen to obtain *engineering* results in a reasonable time frame. The accuracy of such a resolution choice obviously requires confirma-

(c)1999 American Institute of Aeronautics & Astronautics

tion using both comparison with experimental data and higher grid resolution LES results. In the present paper, we demonstrate the current LES capability by direct comparison with data. Higher grid resolution LES is deferred to a future study.

The initial conditions for nonreacting LES were set approximately using turbulent jet profiles and, therefore, a period of time was required to wash the initial conditions out before accurate data can be collected. The inflow conditions were specified based on the information provided by GEAE and University of Illinois at Urbana-Champaign (UIUC). The normalized inflow velocity profiles (axial, radial, and azimuthal) are shown in Figure 3(a). An inflow turbulent field was generated by specifying the given turbulence intensity profile (the incoming intensity of 7%) on randomly generated Gaussian velocity fields. Figure 3(b) shows the inlet equivalence ratio (Φ) profile. The profile indicates a fuel-rich annulus emanating from the outer regions of the premixer exit. Based on this inlet equivalence ratio profile, the inlet fuel species mass fraction (Y_F) distribution has been prescribed: $Y_F = \Phi/(\Phi + (A/F)_{stoic})$ where $(A/F)_{stoic}$ is the stoichiometric air-fuel ratio. In the present study, methane (CH_4) fuel is assumed and, therefore, $(A/F)_{stoic}$=17.12. In LES, the actual inlet equivalence ratio profile is smoother than the measured profile due to the limitation of grid resolution. About 24 grid cells were used to resolve one half of the premixer exit diameter. At the combustor exit, characteristic outflow boundary conditions[33] were imposed. To prevent reverse flow (which will adversely affect the characteristic outflow boundary conditions) from appearing near the outflow, a buffer region was added and its area was linearly contracted by 25% (this buffer extension at the exit is shown in Figure 2).

One arbitrarily chosen instantaneous vorticity-magnitude contour plots obtained from the LES are shown in Figure 4. The plots include one plane perpendicular to z-axis through the combustor centerline (i.e., side view) and three planes perpendicular to x-axis (i.e., end views) at three different downstream locations from the premixer exit (x/D_0=0.25, 0.88, and 1.50, respectively). The swirling incoming premixed jet expands rapidly. The unsteadiness of the flow can be clearly seen in the plots. Detailed animated visualization of the flow field shows that high swirl results in a very complex vortex shedding pattern with significant azimuthal structures. The shear layer is quickly broken up into highly (azimuthally) stretched vortex rings. As the vortices impact on the wall, secondary vortices of the opposite sign are also generated. This phenomenon is well known.

Figure 4 also shows instantaneous contours of the fuel/air distribution (local equivalence ratio) at the same locations. This kind of instantaneous field information is useful in understanding how unmixedness affects NOx generation and degrades flame stability. Moreover, experimental studies[34] showed that temporal unmixedness of the local fuel/air ratio is critical and, in many cases, more significant than time-averaged spatial variations. Therefore, resolution of both spatial and temporal fluctuations are required to accurately predict emissions characteristics in gas turbine combustors. However, experiments are limited in that a whole combustor flow field can not be probed simultaneously. On the other hand, LES can provide any instantaneous field information at any instants.

To obtain statistically stationary results for comparison with the PLIF data provided by UIUC, the LES results were time-averaged for over 10 flow-through times based on the mean centerline axial velocity at the inlet. (Ensemble-average also has been taken along another homogeneous direction, i.e., azimuthal direction, to ensure the achievement of the statistically stationary results.) However, the actual simulation was carried out for over 60 flow-through times to verify that the solution has reached stationary state and it was concluded that the flow has reached stationary state after 10-20 flow-through times. The key limiting condition for such long simulations is the availability of CPU time. The current simulations were carried out on distributed memory parallel processing computers (in particular, the Cray T3E) using the Message-Passing Interface (MPI). MPI is a standard that is available on many machines. Porting computer codes to different machines using MPI is becoming almost routine. The parallelization strategy for the present LES code can be found elsewhere.[4] Typically, 120 processors (of the Cray T3E) were employed primarily to reduce the turn-around time. As demonstrated earlier,[4] the present LES code does scale-up very well on the Cray T3E. A typical simulation using half million grid points on the Cray T3E required about 2 gigabytes of Memory and about 700 single processor hours per flow-through time. Using 120-processors, it was possible to get one flow-through time within 6 (real time) hours.

Figure 5 shows the time-averaged mixing results. At the premixer exit, the variation in the local equivalence ratio across the radius of the premixer was 0.36. This variation has been reduced to 0.15 and 0.09 at locations 12mm and 42mm downstream of the premixer exit surface, respectively. Also, the mixture has become nearly homogeneous (the variation was less than 0.05) at the 72mm axial location. This indicates an order of magnitude decay in time-averaged spatial variations within an axial distance of 1.5 premixer exit diameters. Similar decay has been observed in the experiments by Frazier *et al.*[1]

Figure 6 shows a comparison of the point histogram of equivalence ratio between the experimental data measured by Frazier *et al.*[1] and the LES results using the gradient-diffusion subgrid mixing model. A lay-

(c)1999 American Institute of Aeronautics & Astronautics

out of the positions chosen for the analysis is shown is Figure 1. Frazier *et al.*[1] used only 60 samples at each location to obtain this result (currently, they are reconducting the experiment to improve the result by doubling the number of samples collected). On the other hand, we have used 12000 samples at each location to obtain the LES pdf. As mentioned earlier, pockets containing fuel-rich mixtures emanate from the outer regions of the premixer exit. The broad equivalence ratio distributions of the point histogram along the edge of the premixer exit (location d) exemplify the fluctuating nature of these pockets. Flow reversal and turbulent mixing was sufficient to produce a uniform mixture concentration in the recirculation regions near the premixer exit surface corner (location g). Major difference between the experimental and the LES histograms appears downstream of this location (i.e., locations h and i). LES results show that this uniform mixture concentration persists at the downstream locations while the histograms from the experiment were broadened. Other than this difference, agreement between the experimental data and the LES results is reasonable.

Temporal fluctuations of the local equivalence ratio (i.e., broadness of the histogram) can be quantified using the unmixedness parameter s:

$$s = \frac{\sigma_\Phi}{\mu_\Phi} \tag{16}$$

where μ_Φ and σ_Φ are the time-averaged mean and standard deviation of the local equivalence ratio, respectively. Figure 7 shows the unmixedness parameter s profiles across the radius of the combustor at three downstream locations. As observed in the previous histograms, the agreement between the LES results and the experimental data is reasonablely good at the first downstream locations (i.e., x=12mm). However, at the other two locations, the difference between two data is discernible except for the first radial station (i.e., centerline) comparison. LES predicts the higher mixedness at those locations. One possible explanation for this disagreement is that the contracted buffer region which was attached at the end of the combustor (see Figure 2) to prevent reverse flow near the outflow may have changed the recirculation pattern inside the combustor. Escudier and Keller[35] have experimentally proved that the exit contraction can strongly influence the character of the recirculation zone. Therefore, to improve the simulation accuracy, we may need to include the actual combustor exit conditions which are not presently available (and it may not be easy to implement numerically even if they are available).

Two temporal averages are defined for statistical reduction of data: Reynolds and Favre. Consider the temporally and spatially varying dependent variable $\phi(x_i,t)$. Its Reynolds time average is $\bar{\phi}(x_i) = \int_t^{t+T} \phi(x_i,t')dt'/T$. And, its Favre (density-weighted) average is $\widetilde{\phi(x_i)} = \int_t^{t+T} \bar{\rho}\phi(x_i,t')dt'/(\bar{\rho}T)$, therefore, $\phi(x_i,t) = \widetilde{\phi(x_i)} + \phi'''(x_i,t)$. Figure 8 shows the scalar dissipation rate field $(\partial\widetilde{Y_F}/\partial x_i)(\partial\widetilde{Y_F}/\partial x_i)$ which has been obtained by taking differentiation of (temporal) Favre-averaged fuel species field $\widetilde{Y_F}$. This dissipation field information can provide us the local rate at which the (time-averaged) scalar energy $\widetilde{Y_F}\,\widetilde{Y_F}/2$ is being reduced by molecular diffusion in the flow. In the figure, the peak scalar dissipation rate regions are marked by (x).

The turbulent flux that appears as an unclosed term in the (temporal) Favre-averaged species equation accounts for the turbulent diffusion of scalars and must be modeled. It is common to assume a gradient diffusion model,

$$\bar{\rho}\widetilde{u_i'''Y_m'''} = -\frac{\bar{\rho}\nu_t^R}{Sc_t}\frac{\partial\widetilde{Y_m}}{\partial x_i} \tag{17}$$

where ν_t^R is the eddy viscosity for the Reynolds stress tensor $R_{ij} = \bar{\rho}\widetilde{u_i'''u_j'''}$. A similar assumption has been employed to model the subgrid species transport term $\Phi_{i,m}^{sgs}$ as shown in equation (15). However, the presence of counter-gradient diffusion in turbulent premixed combustion has been well established in theory,[36] experiments,[37,38] and numerical simulations.[9,39,40] Figure 9 shows the turbulent flux $\bar{\rho}\widetilde{u_i'''Y_m'''}$ multiplied by the species gradient $\partial\widetilde{Y_m}/\partial x_i$ and, hereafter, this parameter will be denoted by Υ. Note that, here, x_i is a Cartesian coordinate component and only the fuel species cases are presented. Figure 9 shows x and y-components (i.e., i=1,2) of Υ and z-component is omitted since it behaves similarly with y-component. The parameter Υ itself does not contain any physical significance, however its sign can reveal the appropriateness of the gradient diffusion assumption used in equation (17). In the figure, distinguished regions of a particular sign of Υ are marked by $(-)$ or $(+)$ according to the actual sign of the parameter there. Negative Υ value means that the turbulent flux $\bar{\rho}\widetilde{u_i'''Y_m'''}$ is of gradient type (i.e., same sign with the species gradient $\partial\widetilde{Y_m}/\partial x_i$) while positive Υ value denotes counter-gradient of the turbulent flux. As shown in the figure, x-component of the turbulent flux is of gradient type $(-)$ throughout the flow field. However, for y-component (and similarly z-component), both counter-gradient $(+)$ and gradient $(-)$ diffusions exist. This result clearly demonstrates that even LES employing the subgrid mixing model which is based on the gradient diffusion assumption is capable of capturing the counter-gradient diffusion. This is mainly because counter-gradient transport is a large scale

(c)1999 American Institute of Aeronautics & Astronautics

phenomena[41] and in the LES methodology, the large scales are directly computed.

Figures 10(a)-(f) show, respectively, the nondimensionalized mean axial velocity, the radial velocity, and the tangential velocity profiles along the axial and radial locations. Each figure includes three different radial (or downstream) locational profiles. The experimental data for the mean velocities and turbulent fluctuations are not available for the comparisons and, therefore, these results are evaluated only in a qualitative manner. Vortex breakdown along the centerline is not observed (i.e., mean axial velocity along the centerline remains positive throughout the combustor). Instead, off-centerline recirculation is observed and its front edge is located near location e in Figure 1. Recirculation is likely responsible for broadening of histograms and at location e the experimental histogram is broader than the LES histogram. This means that the location of the off-centerline recirculation predicted by the LES is little off from the experimental data or its strength is little weaker than the data. The mean radial velocity profiles show that this component decays quickly and vanishes within an axial distance of one premixer exit diameter. On the other hand, the mean tangential velocity component is still significant even at the combustor exit.

Figures 11(a)-(f) show similar plots for the root-mean-square (RMS) of the fluctuating components. Most interesting feature observed from these figures is that the radial component of turbulent fluctuations is the most energetic while its mean contains the least energy (see Figure 10). The transient variation of all three component fluctuation levels has disappeared within an axial distance of one premixer exit diameter.

Figures 12(a)-(f) show, respectively, the model coefficient C_ν, the dissipation model coefficient C_ε, and the subgrid kinetic energy profiles also along both the axial and radial locations. The axial variation of these quantities also has been settled down within an axial distance of one premixer exit diameter. The stationary value (i.e., 0.7-1.0) for C_ν is significantly larger than the C_ν value obtained from incompressible turbulent flow simulations. Kim and Menon[6] obtained $C_\nu \cong 0.55$ from LES of turbulent Couette flows using the incompressible version of the LDKM. To determine whether the larger C_ν is required for the present study, LES using the constant coefficient model has been carried out and we were able to stabilize the simulation only when $C_\nu > 1.0$. The value and the variation of C_ε across the combustor are similar to those observed from the incompressible LES. The subgrid kinetic energy is nondimensionalized using the kinetic energy based on the mean centerline axial velocity at the inlet (i.e., $K_0 = U_0^2/2$). The axial profiles of subgrid kinetic energy (and also C_ν and C_ε) change rapidly within 5mm downstream of the premixer exit and seem to adjust themselves to an adequate level. The radial profiles of the subgrid kinetic energy behaves similarly as those of the tangential turbulent fluctuations.

5 CONCLUSIONS

This paper has reported on the application of LES to turbulent fuel/air mixing in a gas turbine combustor that is a close approximation of a lean premixed combustor under development at General Electric Aircraft Engine Company. The eventual goal of this ongoing study is to develop the computational methodology which can quantify the efficiency of the premixer of gas turbine combustors. As the first step toward achieving this eventual goal, the present study was focussed on evaluating the current capability of LES methodology which employs a conventional subgrid mixing model. The LES methodology has been used to predict the unmixedness observed in the experiments and it also has been used to obtain detailed information related to the scalar properties which may not be obtainable from experiments. In particular, LES has been carried out to determine whether it can capture the experimentally observed phenomenon that the swirling fuel/air mixture generated by the dual annular counter-rotating premixer has significant spatial variation in the local equivalence ratio in the near field. This unmixedness can impact the emission characteristics of the combustor. Comparison of the computed results with experimental data indicated reasonably good agreement in spite of a simple subgrid mixing model and relatively coarse grid resolution employed in the LES. Some discrepancy of the comparisons with data in the downstream region still remains to be resolved. If the agreement remains poor even after more samples are experimentally obtained (as is planned), then this might suggest the need to develop and implement a more comprehensive subgrid scalar model. Such an effort is already underway and results will be reported soon.[30]

6 Acknowledgments

We wish to thank Professor J. E. Peters for providing the experimental data. This work was supported in part by the Army Research Office Multidisciplinary University Research Initiative grant DAAH04-96-1-0008. Computations were carried out under the DoD HPC Grand Challenge Project at NAVO, Stennis Space Center and ARC, Huntsville.

References

[1] Frazier, T. R., Foglesong, R. E., Coverdill, R. E., Peters, J. E., and Lucht, R. P., "An Experimental Investigation of Fuel/Air Mixing in an Optically Accessible Axial Premixer," *AIAA-98-3543*, 1998.

[2] Fric, T. F., "Effects of Fuel-Air Unmixedness on NOx Emissions," *Journal of Propulsion and Power*, Vol. 9, No. 5, 1993, pp. 708–713.

(c)1999 American Institute of Aeronautics & Astronautics

[3] Shih, W. P., Lee, J. G., and Santavicca, D. A., "Stability and Emissions Characteristics of a Lean Premixed Gas Turbine Combustor," *Twenty-Sixth Symposium (International) on Combustion*, 1996.

[4] Kim, W.-W., Menon, S., and Mongia, H. C., "Large-Eddy Simulation of a Gas Turbine Combustor Flow," *Combustion Science and Technology* (to appear).

[5] Kim, W.-W. and Menon, S., "A New Dynamic One-Equation Subgrid-Scale Model for Large-Eddy Simulations," *AIAA-95-0356*, 1995.

[6] Kim, W.-W. and Menon, S., "An Unsteady Incompressible Navier-Stokes Solver for Large-Eddy Simulation of Turbulent Flows," *International Journal for Numerical Methods in Fluids* (to appear).

[7] Menon, S. and Calhoon, W., "Subgrid Mixing and Molecular Transport Modeling for Large-Eddy Simulations of Turbulent Reacting Flows," *Twenty-Sixth Symposium (International) on Combustion*, 1996, pp. 59–66.

[8] Calhoon, W. H. and Menon, S., "Linear-Eddy Subgrid Model for Reacting Large-Eddy Simulations: Heat Release Effects," *AIAA-97-0368*, 1997.

[9] Smith, T. M. and Menon, S., "Subgrid Combustion Modeling for Premixed Turbulent Reacting Flows," *AIAA-98-0242*, 1998.

[10] Erlebacher, G., Hussaini, M. Y., Speziale, C. G., and Zang, T. A., "Toward the Large-Eddy Simulation of Compressible Turbulent Flows," *Journal of Fluid Mechanics*, Vol. 238, 1992, pp. 155–185.

[11] Menon, S., Yeung, P.-K., and Kim, W.-W., "Effect of Subgrid Models on the Computed Interscale Energy Transfer in Isotropic Turbulence," *Computers and Fluids*, Vol. 25, No. 2, 1996, pp. 165–180.

[12] Germano, M., Piomelli, U., Moin, P., and Cabot, W. H., "A Dynamic Subgrid-Scale Eddy viscosity Model," *Physics of Fluids A*, Vol. 3, No. 11, 1991, pp. 1760–1765.

[13] Spyropoulos, E. T. and Blaisdell, G. A., "Evaluation of the Dynamic Subgrid-Scale Model for Large-Eddy Simulations of Compressible Turbulent Flows," *AIAA-95-0355*, 1995.

[14] Najjar, F. M. and Tafti, D. K., "Study of Discrete Test Filters and Finite Difference Approximations for the Dynamic Subgrid-Scale Stress Model," *Physics of Fluids*, Vol. 4, No. 8, 1996, pp. 1076–1088.

[15] Schumann, U., "Subgrid Scale Model for Finite Difference Simulations of turbulent Flows in Plane Channels and Annuli," *Journal of Computational Physics*, Vol. 18, 1975, pp. 376–404.

[16] Liu, S., Meneveau, C., and Katz, J., "On the Properties of Similarity Subgrid-Scale Models as Deduced from Measurements in a Turbulent Jet," *Journal of Fluid Mechanics*, Vol. 275, 1994, pp. 83–119.

[17] Lilly, D. K., "A Proposed Modification of the Germano Subgrid-Scale Closure Method," *Physics of Fluids A*, Vol. 4, No. 3, 1992, pp. 633–635.

[18] Cabot, W. H. and Moin, P., "Large Eddy Simulation of Scalar Transport with the Dynamic Subgrid-Scale Model," *LES of Complex Engineering and Geophysical Flows*, edited by B. Galperin and S. Orszag, Cambridge University Press, 1993, pp. 141–158.

[19] Lund, T. S., Ghosal, S., and Moin, P., "Numerical Experiments with Highly-Variable Eddy Viscosity Models," *Engineering Applications of Large Eddy Simulations*, edited by U. Piomelli and S. Ragab, Vol. 162 of *FED*, ASME, 1993, pp. 7–11.

[20] Wong, V. C., "A Proposed Statistical-Dynamic Closure Method for the Linear or Nonlinear Subgrid-Scale Stresses," *Physics of Fluids A*, Vol. 4, No. 5, 1992, pp. 1080–1082.

[21] Fureby, C., Tabor, G., Weller, H. G., and Gosman, A. D., "A Comparative Study of Subgrid Scale Models in Homogeneous Isotropic Turbulence," *Physics of Fluids*, Vol. 9, No. 5, 1997, pp. 1416–1429.

[22] Schumann, U., "Realizability of Reynolds-Stress Turbulence Models," *The Physics of Fluids*, Vol. 20, No. 5, 1976, pp. 721–725.

[23] Fureby, C., "Towards Large Eddy Simulations of Flows in Complex Geometries," *AIAA-98-2806*, 1998.

[24] Kim, W.-W., *A New Dynamic Subgrid-Scale Model for Large-Eddy Simulation of Turbulent Flows*, Ph.D. thesis, Georgia Institute of Technology, Atlanta, GA, September 1996.

[25] Menon, S. and Kim, W.-W., "High Reynolds Number Flow Simulations Using the Localized Dynamic Subgrid-Scale Model," *AIAA-96-0425*, 1996.

[26] Kim, W.-W. and Menon, S., "Application of the Localized Dynamic Subgrid-Scale Model to Turbulent Wall-Bounded Flows," *AIAA-97-0210*, 1997.

[27] Nelson, C. C. and Menon, S., "Unsteady Simulations of Compressible Spatial Mixing Layers," *AIAA-98-0786*, 1998.

(c)1999 American Institute of Aeronautics & Astronautics

[28] Frankel, S. H., Adumitroaie, V., Madnia, C. K., and Givi, P., "Large Eddy Simulation of Turbulent Reacting Flows by Assumed pdf Methods," *Engineering Applications of Large Eddy Simulations*, edited by U. Piomelli and S. Ragab, Vol. 162 of *FED*, ASME, 1993, pp. 81–101.

[29] Menon, S., McMurtry, P., and Kerstein, A. R., "A Linear Eddy Mixing Model for Large Eddy Simulation of Turbulent Combustion," *LES of Complex Engineering and Geophysical Flows*, edited by B. Galperin and S. Orszag, Cambridge University Press, 1993.

[30] Kim, W.-W. and Menon, S., "Numerical Modeling of Fuel/Air Mixing in a Dry Low-Emission Premixer," Second AFOSR International Conference on DNS and LES, Rutgers University, June 7-9, 1999 (to be presented).

[31] Joshi, N. D., Mongia, H. C., Leonard, G., Stegmaier, J. W., and Vickers, E. C., "Dry Low Emissions Combustor Development," *ASME-98-GT-310*, 1998.

[32] Joshi, N. D., Epstein, M. J., Durlak, S., Marakovits, S., and Sabia, E., "Development of a Fuel Air Premixer for Aero-Derivative Dry Low Emissions Combustors," *ASME-94-GT-253*, 1994.

[33] Poinsot, T., Echekki, T., and Mungal, M. G., "A Study of the Laminar Flame Tip and Implications for Premixed Turbulent Combustion," *Combustion Science and Technology*, Vol. 81, 1992, pp. 45–73.

[34] Mongia, R. K., Tomita, E., Hsu, F. K., Talbot, L., and Dibble, R. W., "Use of an Optical Probe for Time-Resolved in Situ Measurements of Local Air-to-Fuel Ratio and Extent of Fuel Mixing with Applications to Low NOx Emissions in Premixed Gas Turbines," *Twenty-Sixth Symposium (International) on Combustion*, 1996.

[35] Escudier, M. P. and Keller, J. J., "Recirculation in Swirling Flow: A Manifestation of Vortex Breakdown," *AIAA Journal*, Vol. 23, No. 1, 1985, pp. 111–116.

[36] Libby, P. A. and Bray, K. N. C., "Countergradient Diffusion in Premixed Turbulent Flames," *AIAA Journal*, Vol. 19, No. 2, 1981, pp. 205–213.

[37] Cho, P., Law, C. K., Cheng, R. K., and Shepherd, I. G., "Velocity and Scalar Fields of Turbulent Premixed Flames in Stagnation Flow," *Twenty-Second Symposium (International) on Combustion*, 1988, pp. 739–745.

[38] Li, S. C., Libby, P. A., and Williams, F. A., "Experimental Investigation of a Premixed Flame in an Impinging Turbulent Stream," *Twenty-fifth Symposium (International) on Combustion*, 1994, pp. 1207–1214.

[39] Veynante, D., Trouvé, A., Bray, K. N. C., and Mantel, T., "Gradient and Counter-Gradient Scalar Transport in Turbulent Premixed Flames," *Journal of Fluid Mechanics*, Vol. 332, 1997, pp. 263–293.

[40] Veynante, D. and Poinsot, T., "Effects of Pressure Gradients on Turbulent Premixed Flames," *Journal of Fluid Mechanics*, Vol. 353, 1997, pp. 83–114.

[41] Bray, K. N. C., "Turbulent Transport in Flames," *Proceedings of the Royal Society of London A*, Vol. 451, 1995, pp. 231–256.

(c)1999 American Institute of Aeronautics & Astronautics

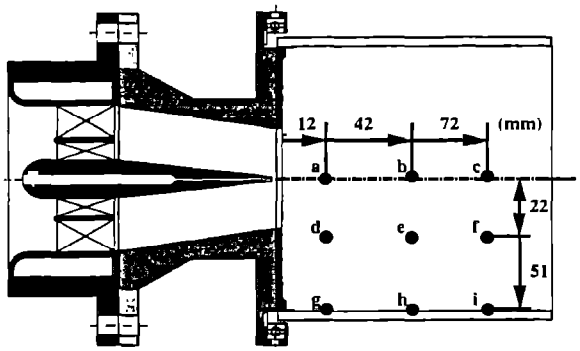

Fig. 1 Centerline sectional view of the dry low NOx gas turbine combustor.

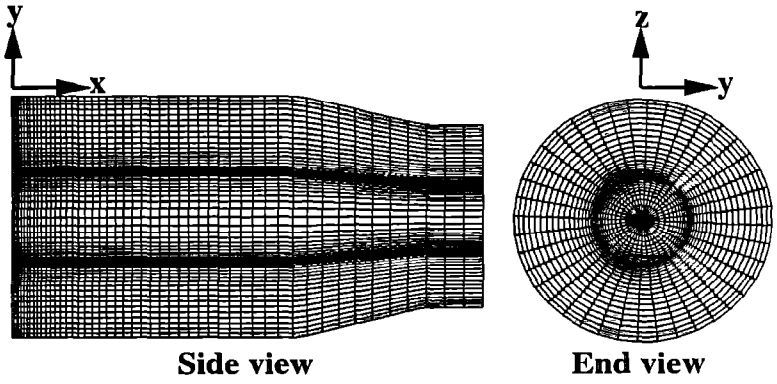

Fig. 2 *Computational grid.*

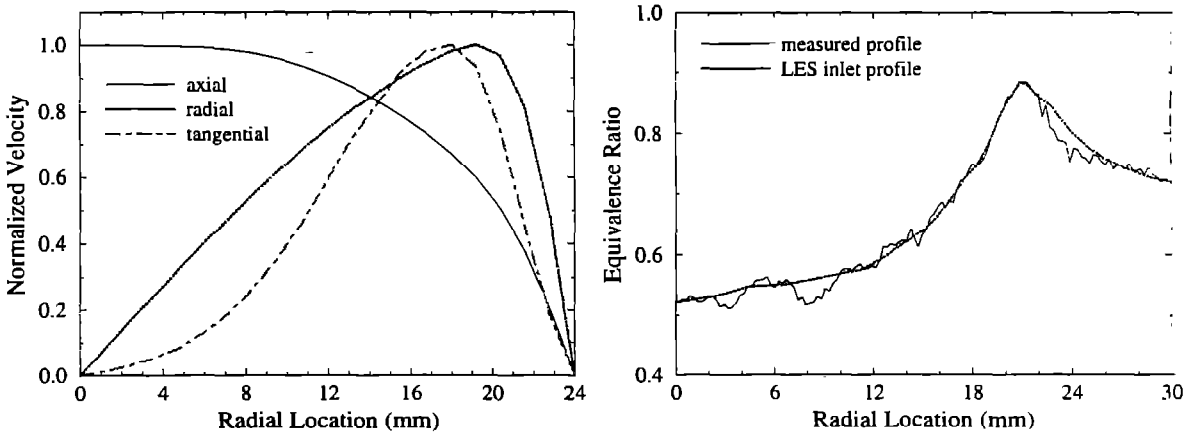

a) Normalized inflow velocity profiles

b) Inlet equivalence ratio profile

Fig. 3 Inflow conditions.

(c)1999 American Institute of Aeronautics & Astronautics

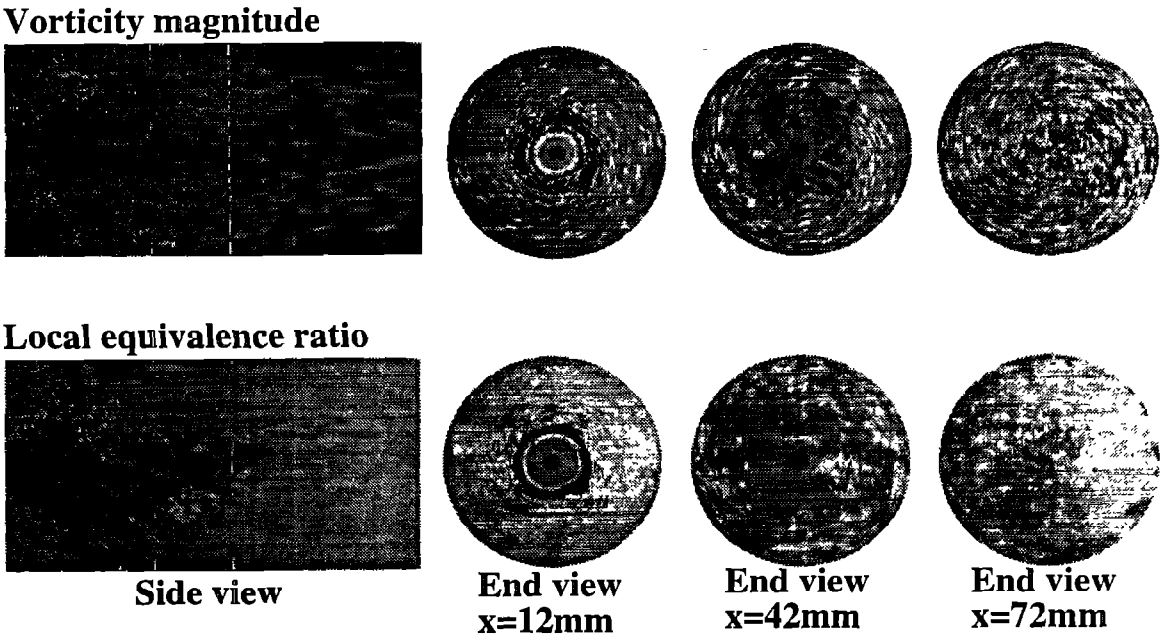

Fig. 4 Instantaneous vorticity magnitude and local equivalence ratio contours.

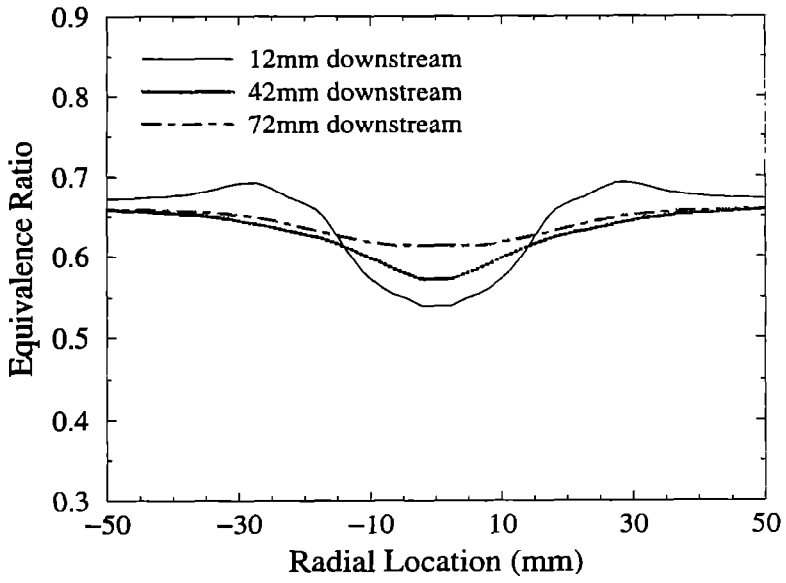

Fig. 5 Radial profiles of the time-averaged local equivalence ratio.

(c)1999 American Institute of Aeronautics & Astronautics

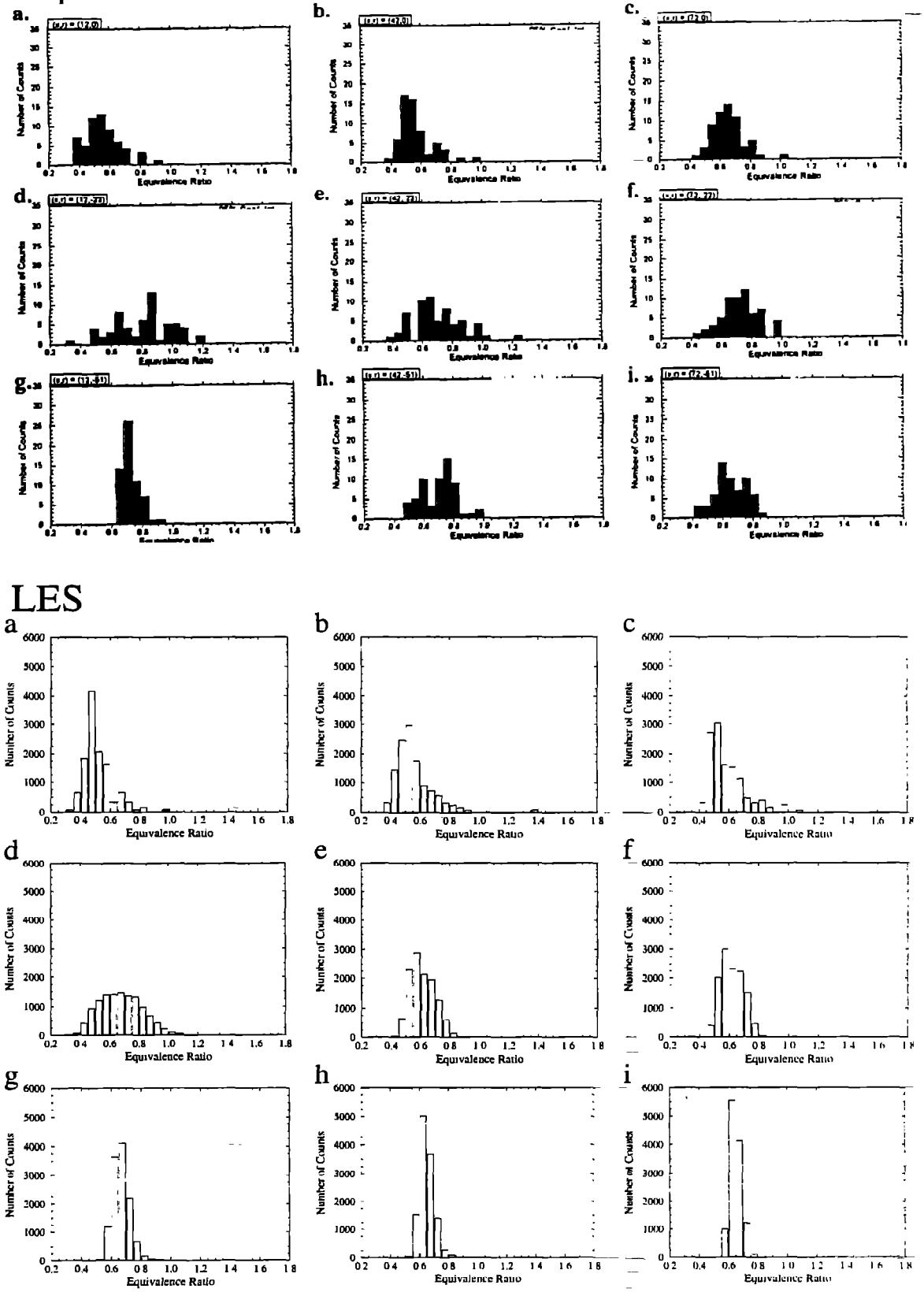

Fig. 6 Comparison of the point histograms of equivalence ratio.

(c)1999 American Institute of Aeronautics & Astronautics

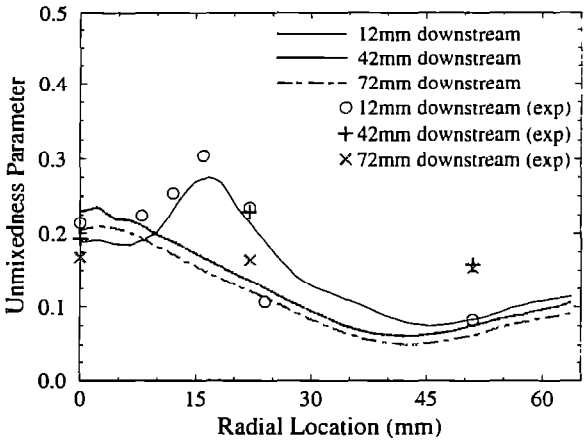

Fig. 7 Radial profiles of the unmixedness parameter s.

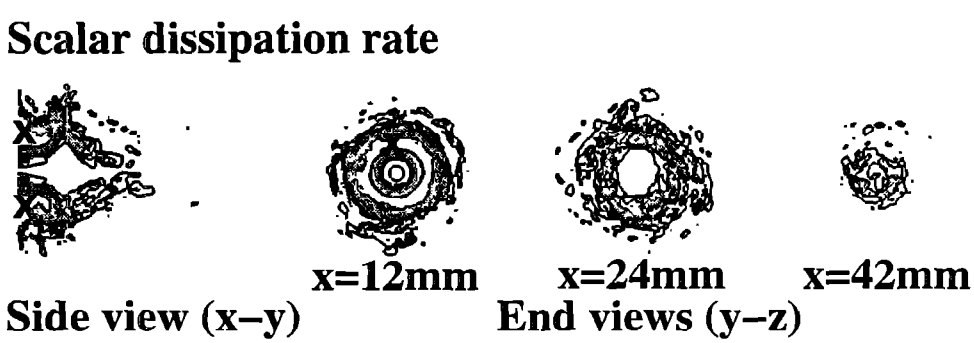

Fig. 8 Scalar (Favre-averaged fuel species) dissipation rate contours.

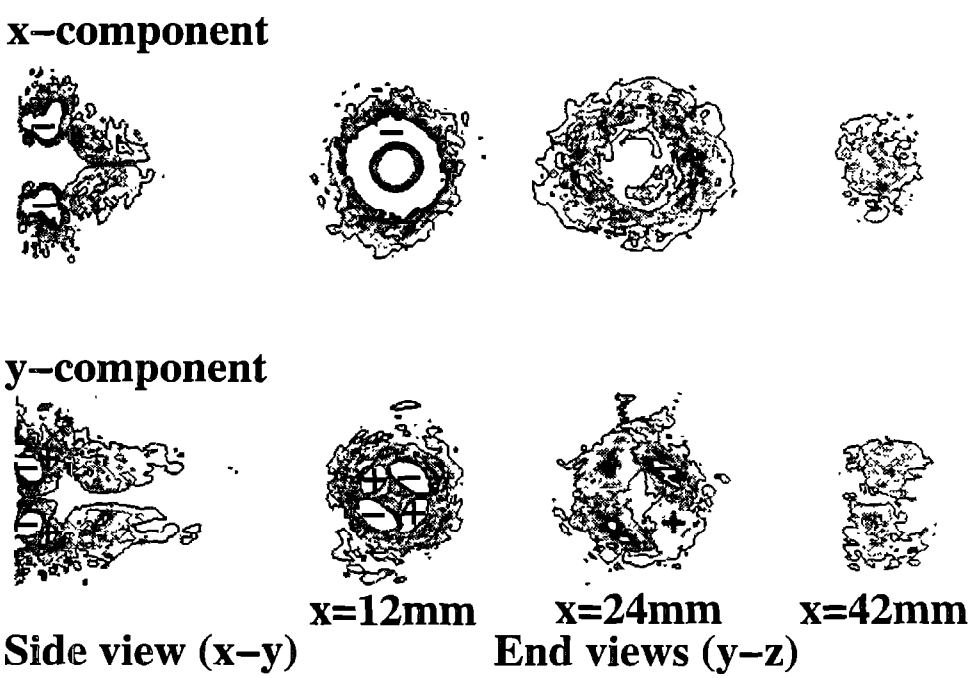

Fig. 9 Contours of Υ.

(c)1999 American Institute of Aeronautics & Astronautics

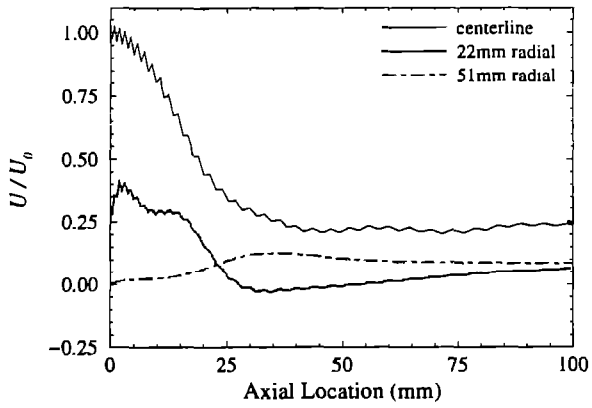

a) Axial profiles of the mean axial velocity component

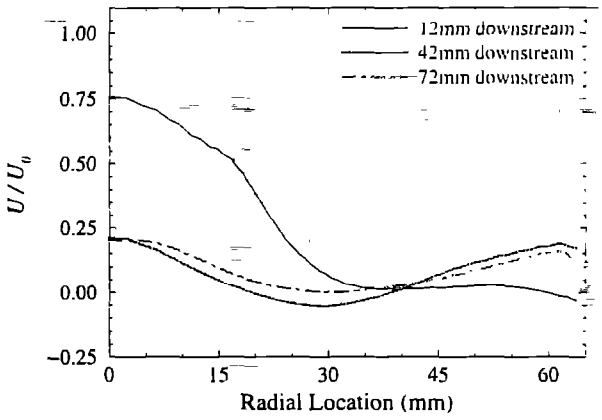

b) Radial profiles of the mean axial velocity component

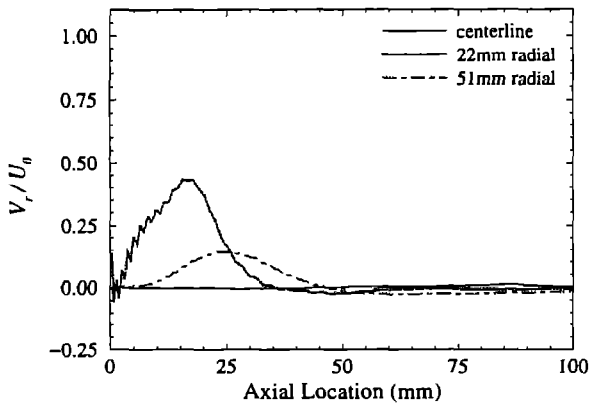

c) Axial profiles of the mean radial velocity component

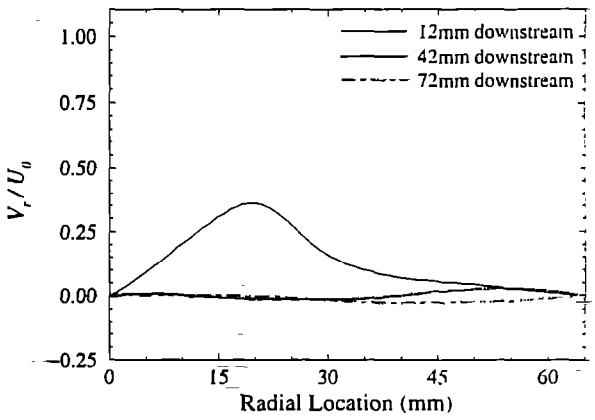

d) Radial profiles of the mean radial velocity component

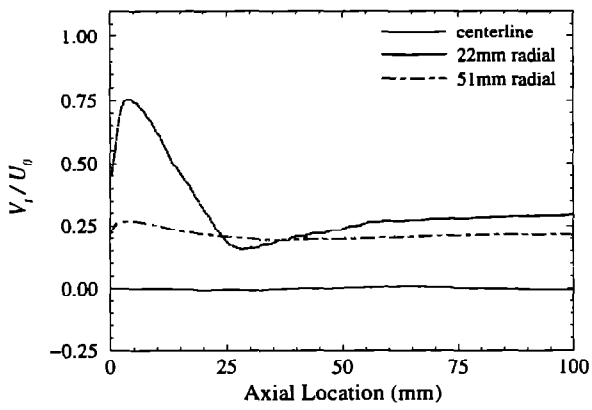

e) Axial profiles of the mean tangential velocity component

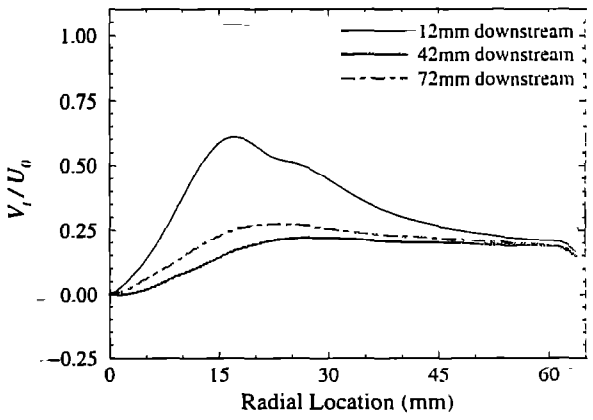

f) Radial profiles of the mean tangential velocity component

Fig. 10 Nondimensionalized mean velocity profiles.

(c)1999 American Institute of Aeronautics & Astronautics

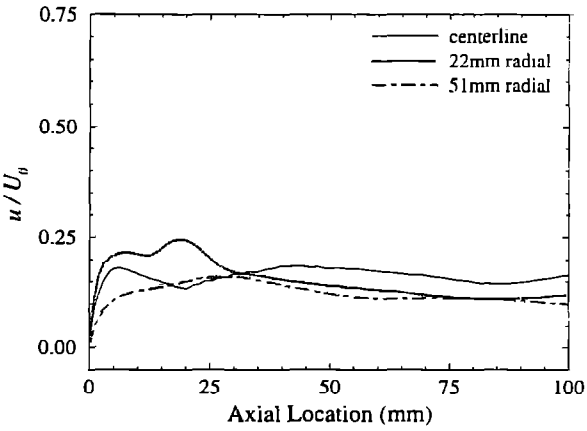

a) Axial profiles of the axial turbulence intensity component

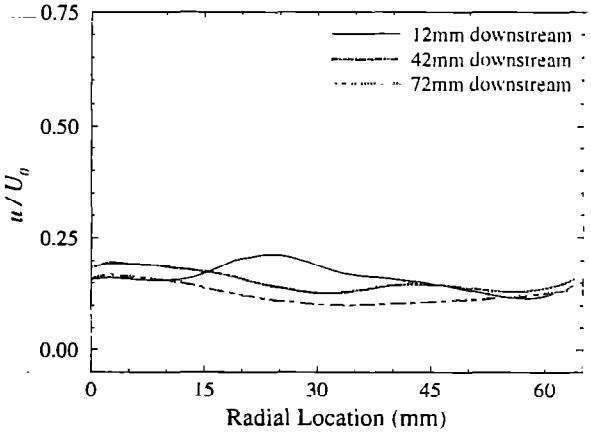

b) Radial profiles of the axial turbulence intensity component

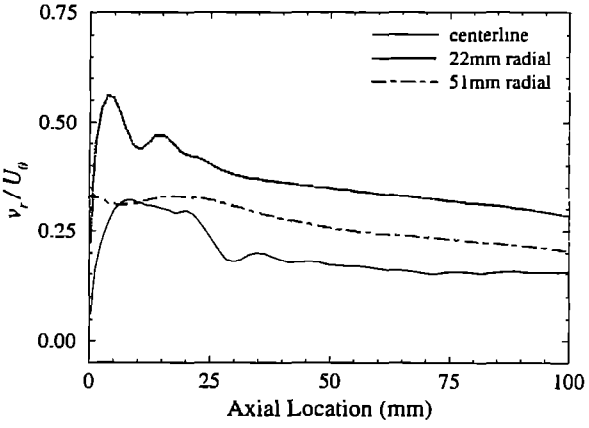

c) Axial profiles of the radial turbulence intensity component

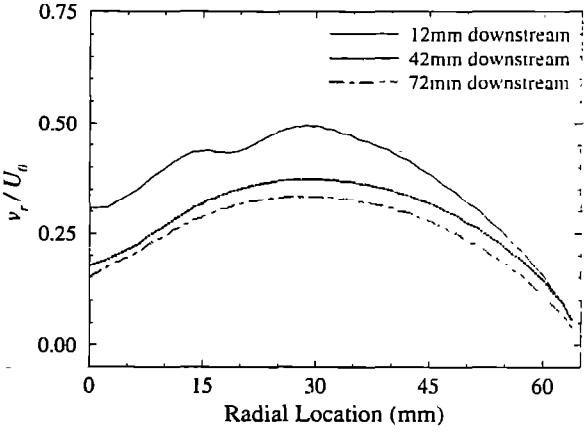

d) Radial profiles of the radial turbulence intensity component

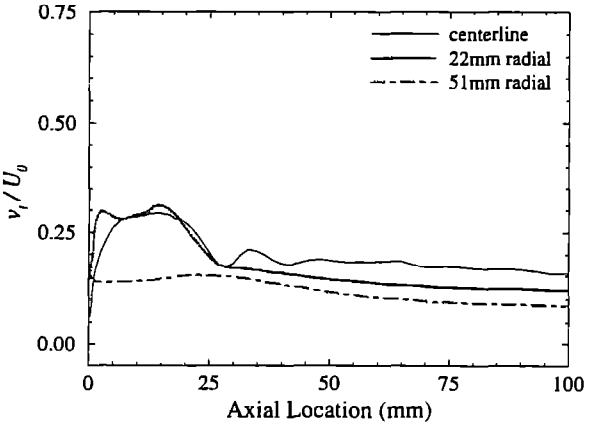

e) Axial profiles of the tangential turbulence intensity component

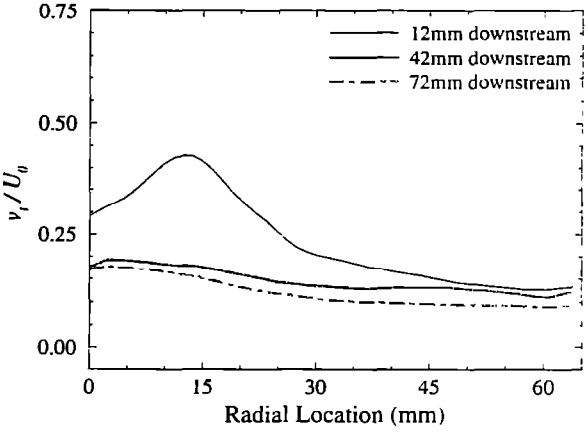

f) Radial profiles of the tangential turbulence intensity component

Fig. 11 Nondimensionalized turbulence intensity profiles.

(c)1999 American Institute of Aeronautics & Astronautics

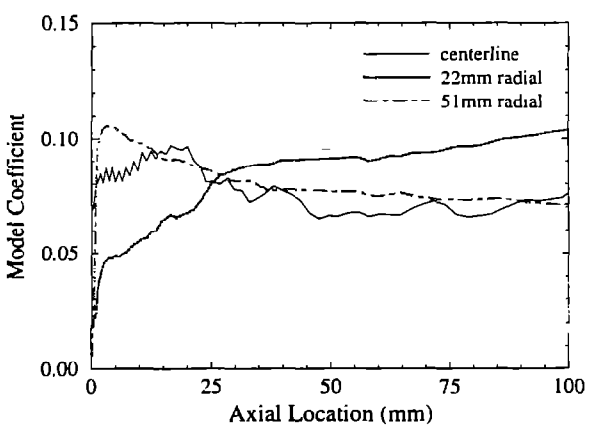

a) Axial profiles of C_ν

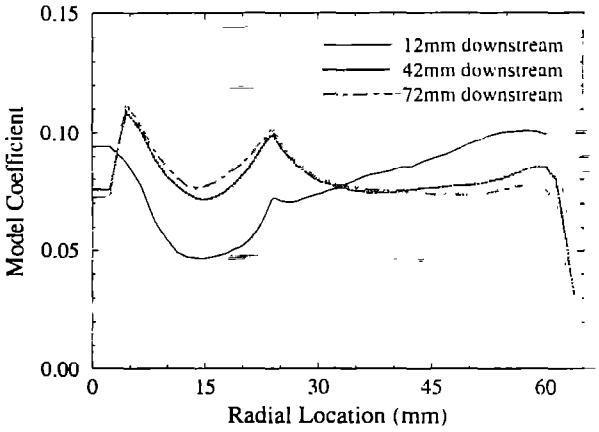

b) Radial profiles of C_ν

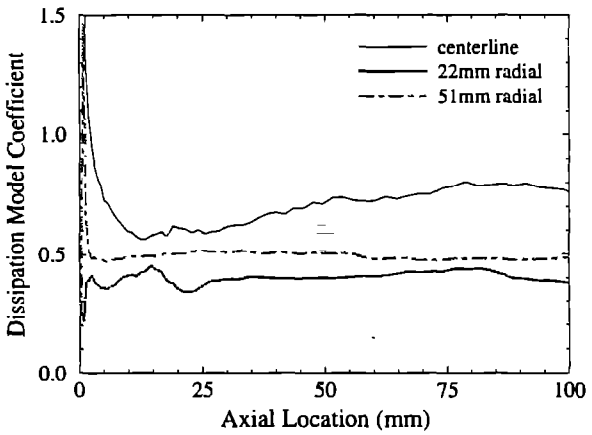

c) Axial profiles of C_ϵ

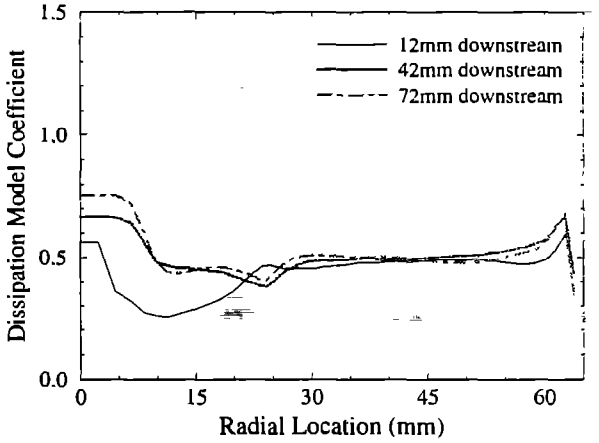

d) Radial profiles of C_ϵ

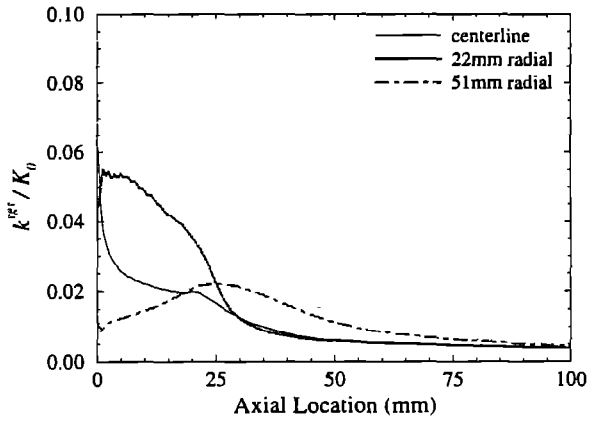

e) Axial profiles of k^{sgs}

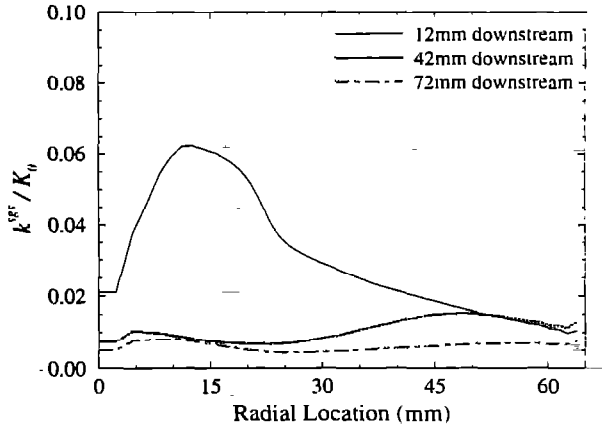

f) Radial profiles of k^{sgs}

Fig. 12 Time averaged profiles of C_ν, C_ϵ, and the nondimensionalized subgrid kinetic energy.